



ALMA MATER STUDIORUM
UNIVERSITÀ DI BOLOGNA

ARCHIVIO ISTITUZIONALE
DELLA RICERCA

Alma Mater Studiorum Università di Bologna Archivio istituzionale della ricerca

Modeling UAV-Based IoT Clustered Networks for Reduced Capability UEs

This is the final peer-reviewed author's accepted manuscript (postprint) of the following publication:

Published Version:

Mignardi S., Buratti C. (2023). Modeling UAV-Based IoT Clustered Networks for Reduced Capability UEs. IEEE INTERNET OF THINGS JOURNAL, 10(12), 10266-10279 [10.1109/JIOT.2023.3238654].

Availability:

This version is available at: <https://hdl.handle.net/11585/960712> since: 2024-03-06

Published:

DOI: <http://doi.org/10.1109/JIOT.2023.3238654>

Terms of use:

Some rights reserved. The terms and conditions for the reuse of this version of the manuscript are specified in the publishing policy. For all terms of use and more information see the publisher's website.

This item was downloaded from IRIS Università di Bologna (<https://cris.unibo.it/>).
When citing, please refer to the published version.

(Article begins on next page)

Modelling UAV-based IoT Clustered Networks For Reduced Capability UEs

Silvia Mignardi and Chiara Buratti

WiLab, CNIT / DEI, University of Bologna, Bologna, Italy

{silvia.mignardi, c.buratti}@unibo.it

Abstract—In recent years, the use of Unmanned Aerial Vehicles (UAVs) for wireless communications has been shown promising in a plethora of different applications. Their flexible deployment and mobility make them key enablers for the next generation of networks, provided that system design is properly addressed. In this article, we analyze a beyond-5G network where an Unmanned Aerial Vehicle (UAV), acting as Unmanned Aerial Base Station (UAB), is employed to collect data from Reduced Capability User Equipments (UEs), deployed in an urban area. Specifically, we study a cluster-based scenario, where UEs are deployed following a Thomas cluster process, and the UAB flies over cluster centers according to the Traveling Salesman Problem solution. Through the use of a stochastic approach, we mathematically devise the system performance accounting for uplink transmission protocol constraints, random access procedure, finite number of radio resources available, and coverage issues during the UAB flight. The mathematical model, validated via comparison with simulations, allows to optimize some system parameters, like the UAB speed, the number of UEs per cluster and the number of radio resources to be used for the access and for data transmissions.

Index Terms—Internet of Things, Unmanned Aerial Base Stations, RedCap, stochastic modelling.

I. INTRODUCTION

The next generation of wireless networks demands an increasing level of planning and adaptability to new traffic types and use cases. This becomes especially true for Internet of Things (IoT) environments, where the traffic requirements may be very diverse, from machine-type communication with short packet sizes to ultra-reliable and low latency communications, industrial scenarios, and throughput-demanding novel applications (e.g., video monitoring). Nowadays, autonomous unmanned aerial vehicles (UAVs) are gaining attention for a multitude of novel applications [1]–[3], among which, one of the most promising, envisions UAVs providing communication services for collecting data from IoT nodes [4]. In fact, having UAVs with onboard-mounted small base stations (BSs), hereafter denoted as unmanned aerial BSs (UABs), is a feasible approach to increase network flexibility [5].

The use of UABs in IoT scenarios may be very interesting to accommodate bursty traffic or a massive number of simultaneous transmissions, typical of IoT environments [6]–[10], where the diverse application requirements pose several challenges to conventional terrestrial deployments. Indeed, operators can employ UABs only when needed and for a limited time, thus saving energy and maintenance costs. Furthermore, since usually IoT nodes are placed in known and static positions and

the traffic they generate can be easily predicted, the network can make decisions in advance on when and where the UAB is needed, planning its trajectory [11], [12].

The 3rd Generation Partnership Project (3GPP) standardization body is introducing in Rel.17 a new cellular IoT technology characterizing Reduced-Capability (RedCap) user equipments (UEs) for the fifth-generation (5G) New Radio (NR). Use cases for RedCap UEs include urban monitoring or video surveillance, wearable and industrial wireless sensors, extending the capabilities of the previous cellular IoT technologies, but limiting requirements compared to the usual broadband NR UEs [13]. Furthermore, being based on NR, RedCap UEs can take advantage of mm-Wave transmissions in Frequency Range 2 (FR2).

In this article, we consider a UAB in charge of collecting cellular IoT data from RedCap UEs deployed in an urban area. Although the advantages of such systems are promising, several challenges arise. First, the trajectory should be planned in advance to fairly reach all nodes, considering that IoT nodes may not be in line-of-sight. Second, due to the limited battery of the UAV, the connection time between the UAB and an IoT node is limited and trajectory-dependent, causing potential interruptions in the communication or failure in the access procedure. Optimal trade-offs between the number of nodes attempting to access and the number of radio resources available shall be found.

Similarly to other works [11], [14], the focus of this article is not on the UAV trajectory optimization but rather on the definition of a mathematical model that allows deriving the performance of a UAB-aided IoT network by appositely tuning the system parameters (e.g., frame structure, UAB height and speed, access configuration, etc.). The analysis is performed through the use of stochastic geometry, for what concerns the coverage analysis, and queuing theory, for the access probability. To do this, we first analyse a static scenario, where only one cluster is considered, and the UAB is assumed to be stationary and located in the cluster center. Then, we consider an intermediate scenario where the UAB hovers for a predefined time above the same cluster, giving the nodes the possibility to try to access the channel and receive radio resources multiple times. Finally, we move to a fully dynamic scenario, where the UAB follows a predefined trajectory to cover all the clusters. Furthermore, the analysis includes different types of access structures, such as contention-based and contention-free. The model allows to predict the network performance by tuning the protocol and network parameters,

helping the network planning. The mathematical framework is validated via comparison with Monte-Carlo simulations, and the software used in the simulator was built on purpose and made available online at [15].

The paper is organized as follows. Related works are discussed in Sec. II. The system model is introduced in Sec. III, and the protocol access structure together with resource allocation in Sec. IV. Our mathematical approach is reported in Sec. V for the static case with a single attempt, in Sec. VI for the static case with multiple attempts, and in Sec. VII for the dynamic case. The model comparison with simulations is reported in Sec. VIII along with optimization parameters, and conclusions follow in Sec. IX.

II. RELATED WORKS

As the recent advancements in the UAV technology are gaining momentum, a number of studies investigate the use of UAVs for IoT applications, optimizing the deployment, the energy saving, the data offload and the delay constraints [16]–[20]. Initial studies targeting a mathematical description of UAV services focus on coverage analysis [21], [22], show the non-trivial impact of the different aerial channel environments [23], and the impact of interference [24]. A stochastic-based analysis of UAVs serving IoT nodes is reported in [25]; expressions for coverage and data rate under the proposed UAV deployment are provided when using the NarrowBand-Internet of Things (NB-IoT) standard. However, authors did not consider the channel access probability and the case in which the number of nodes competing for the channel is higher than the resources available. Authors in [26] consider the coverage probability, interference, and data rate analysis with an ideal UAV fleet motion to finally assess the harvesting capability of the proposed system. The work in [14] targets wildfire detection from IoT sensors communicating to UAVs. The authors do not focus on trajectory design, as the study targets a lower-bound use case modelling including the fire spread, sensor detection model, and wildfire detection probability. A very interesting protocol-based analysis is presented in [27]; the article assesses the performance of carrier-sense multiple access with collision avoidance (CSMA/CA) in UAV-aided IoT networks, where it considers a quitting probability due to coverage and UAV mobility and proposes an improved CSMA/CA protocol. Furthermore, [28] targets intelligent reflecting surfaces assisted UAV communications for IoT networks, where mainly path loss, Signal-to-Noise ratio (SNR), and symbol error rate are deeply investigated to achieve closed form expressions and analytical bounds. Finally, an age of information study is discussed in [29], where the packet loss rate and data quantity are evaluated using a Markov chain.

However, these works do not account for variations in the number of covered nodes during the UAV flight and do not consider a coverage analysis at mm-Wave. In addition, they lack a protocol-dependent mathematical study that includes: i) channel access probability with the possibility for an IoT node to attempt several times; ii) blocking probability because of limited resources availability. To summarize, our contributions can be listed as follows:

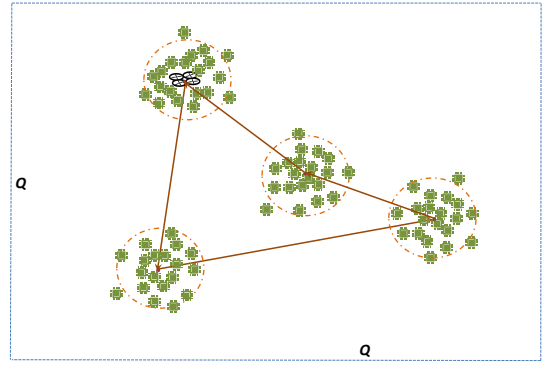


Fig. 1: Reference scenario with TSP trajectory.

- We model the coverage probability of an hovering UAB working in a mm-Wave channel (FR2) to serve clustered IoT nodes;
- Based on the access structures considered by the 3GPP (with or without contention), we infer the access probability, resource availability, and blocking probability;
- We model the impact of moving from a static to a dynamic scenario, where the number of IoT covered by the UAB changes during the flight;
- We derive a number of metrics that define the network performance, such as the transmission success probability and the network throughput.

This article can be considered an extension of [11]. Differently from [11], we i) update the propagation model to consider systems with higher rates and a mm-Wave channel, ii) improve the modelling of the UAV mobility, introducing a new analysis reported in Section VII, iii) consider different access types, together with a blocking probability, and iv) compare the proposed model with Monte-Carlo simulations.

III. SYSTEM MODEL

A. Reference Scenario

We assume one UAB is initially parked next to one battery recharge or replace station, and a number of RedCap UEs, hereafter simply denoted as nodes, is deployed inside the UAB's squared service area having size Q^2 . We assume these IoT nodes are grouped into clusters following a Thomas cluster process (TCP) [30], from the Poisson cluster process (PCP) family. Examples of reference scenarios may be an industrial zone, where sensor nodes implement the 4.0 industry concept, smart buildings, or even areas of service offered by the municipality (e.g., a parking area). In a TCP, the parent points (i.e., the clusters' centers), form a homogeneous Poisson point process (PPP) of intensity λ_p [nodes/m²]. In the following, n_p denotes the number of parent points in the area, which is a Poisson r.v. with mean $\bar{n}_p = \lambda_p Q^2$. Around each parent point, a Poisson number of offspring points, with intensity λ_s [nodes/m²], are deployed according to a symmetric normal distribution with intensity variance σ^2 . The offspring points represent the RedCap UEs. Then, n denotes the number of offspring points per cluster, being a r.v. with mean $\bar{n} = \lambda_s Q^2$.

One UAB is deployed in the scenario to provide network service to the IoT nodes. Nodes are assumed to be outside

the coverage of terrestrial fixed infrastructure and have no stringent latency requirements. In this scenario, one operational UAV is sufficient for the overall nodes' coverage, but its network parameter settings must be carefully planned. A snapshot of the considered scenario is depicted in Fig. 1. Note that, for the scope of this paper, we do not model the consumption of the UAB, that is we assume the capacity of its battery is sufficient to enable a full round trip over any trajectory.

B. Channel Model

In this article, the propagation model affects the UAB-ground node link. Because of the increasing network densification and requests for higher rates as compared to the past, we consider a cellular system working at mm-Wave frequencies, where $f_c = 27$ GHz is the carrier frequency. To this respect, we adopt the radio channel model provided in [31] by the 3GPP, where we refer to the urban macro (UMa) scenario for the parameter setting. According to this model, connections between the drone and nodes can either be line of sight (LoS) or Non-LoS (NLoS). For NLoS links, the signals travel in LoS before interacting with objects located close to the ground, which results in a shadowing effect. By denoting as subscript l to indicate LoS and n to indicate NLoS, the path loss for a transmitter-receiver distance d_{3D} , where d_{2D} is the projected 2D distance, is denoted as $L_l(d_{2D}, h)$ in the LoS case, which happens with probability $p(d_{2D})$, and as $L_n(d_{2D}, h)$ in the NLoS case, which happens with probability $(1 - p(d_{2D}))$.

The probability of being in LoS conditions, $p(d_{2D})$, is expressed by [31] as the following Eq. (1), where we assume the indoor distance of the node (i.e., the distance from the closest wall facing outside) is negligible.

$$p(d_{2D}) = \begin{cases} 1 & \text{if } d_{2D} \leq 18 \\ \frac{18}{d_{2D}} + \exp\left(-\frac{d_{2D}}{63}\right) \left(1 - \frac{18}{d_{2D}}\right) & \text{otherwise} \end{cases} \quad (1)$$

where the node height is less than 13 meters.

Then, the path losses for the different cases of propagation in LoS (Eq. (2)) or NLoS (Eq. (3)), are given by:

$$L_1^* = \begin{cases} 28 + 22 \log_{10}(d_{3D}) + 20 \log_{10}(f_c) & \text{if } d_{2D} \leq d_{BP} \\ 28 + 40 \log_{10}(d_{3D}) + 20 \log_{10}(f_c) \\ \quad - 9 \log_{10}(d_{BP}^2 + (h - h_{ut})^2) & \text{otherwise} \end{cases} \quad (2)$$

$$L_1(d_{2D}, h) = L_1^* + \xi_1$$

$$L_n' = 13.54 + 39.08 \log_{10}(d_{3D}) + 20 \log_{10}(f_c) - 0.6(h_{ut} - 1.5)$$

$$L_n^* = \max(L_1, L_n')$$

$$L_n(d_{2D}, h) = L_n^* + \xi_n \quad (3)$$

where $d_{BP} = 4(h - 1)(h_{ut} - 1)\frac{f_c}{c}$ is denoted as breakpoint distance. $\xi_1 \sim \mathcal{N}(0, \sigma_{\xi_1})$ and $\xi_n \sim \mathcal{N}(0, \sigma_{\xi_n})$ are random variables accounting for shadowing fluctuations [31]. We assume the scenario has no validity constraints for this model.

Then, the coverage analysis depends on a maximum loss threshold for receiving sensitivity, denoted as L_{thr} , depending

on which an IoT node is or is not covered by the UAB and may attempt to access the channel.

C. UAB Trajectory

The path designed for the UAB is usually optimized to provide the requested IoT service to all ground nodes. As analysed in [12], a simple but effective solution - given the scenario considered - is to drive the UAB above each cluster center by following the solution of the Travelling Salesman Problem (TSP) over the TCP parent points. Indeed, the orienteering problem is widely studied in operational research [32] and is particularly suited in such a scenario, where the cluster centers become the reference coordinates. Fig. 1 includes a simple representation of the TSP trajectory with three clusters.

To understand the TSP impact on our model, we define the *cluster area*, hereafter denoted as \mathbf{A}_σ , being a 2D circle centered at a parent point and having radius 2σ , that is the area where 95% of the distribution values lay (see the dotted circles in Fig. 1). Then, we account for the forward and backward movement of the UAB to and from the cluster passing through the cluster center (see Fig. 1). This is done by considering the intersection area between the cluster area and the *UAB coverage area*, hereafter denoted as \mathbf{A}_{cov} , approximated as a circular area of radius $R_{cov} = 2\sigma^1$ (see Section VII).

Finally, to simplify the analysis, we assume clusters are sufficiently far apart, such that when the UAB flies over the area of one cluster, the nodes of the other clusters cannot be covered. This assumption is justified by selecting an appropriate area dimension, Q^2 , with respect to the cluster size, and allows to model the UAB mobility cluster per cluster without the need to solve the entire TSP. The TSP has to be solved in the simulation part, instead, where we use a dynamic programming solver to obtain the exact solution.

IV. ACCESS STRUCTURE AND RADIO RESOURCE ALLOCATION

Since IoT traffic is dominantly uplink [33], [34], we focus hereby on uplink transmissions of the sensor nodes to the UAB. Indeed, each node serves as sampling and collecting environmental or structural information data, to be sent and processed by a central node (e.g., a unit able to process raw data and make it available for end users).

For what concerns the access structure of RedCap UEs, we refer to the cellular network numerology suggested by 3GPP. Thus, the uplink channels where the access procedure takes place are the physical random access channel (PRACH) and physical uplink shared channel (PUSCH). The PRACH is responsible for the start of the access procedure and resource grant request, usually by means of preambles, while the node data transmission happens in the PUSCH. Let us now focus on the access procedure. As for the 5G NR standard is concerned, we have two possible procedures for random access (RA), being contention-based random access (CBRA) and contention-free random access (CFRA) [35]. In this paper,

¹This is an approximation, since random channel fluctuations are present, resulting in coverage footprints that are not circular.

we consider both procedures. Also, we focus on the uplink (UL) exchange for the UAB-user link, where the RA preamble is sent from the UE, followed by its data packet.

A. Random Access Schemes

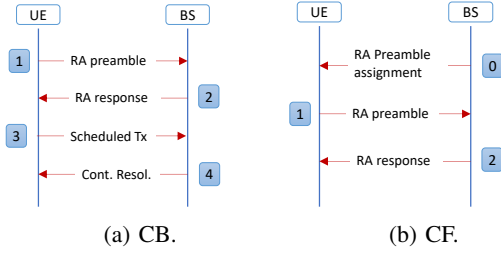


Fig. 2: Message exchange in the 4-step RA for contention-based (CB) and contention-free (CF) schemes [35].

In the contention-based (CB) approach, each node sends an access preamble in a predetermined window (i.e., the PRACH) choosing from a number of available ones, denoted as U_{f_1} . However, other nodes might attempt to access the channel in the same window, and, if anyone selects the same preamble resources, a collision happens. Therefore, the BS (i.e., the UAB) correctly receives the node's UL data with a certain probability, that is the probability the node successfully accesses the channel. The node will be notified of the success of the transmission upon contention resolution messages' reception. In the contention-free (CF) approach, the BS starts the message exchange by assigning resources for the RA preamble and/or UL data. Figure 2 shows the different message exchanges in the CBRA and CFRA schemes.

B. Frame Structure

As we are referring to the 5G NR standard, we assume orthogonal frequency-division multiple access (OFDMA) is used and the resource set is composed of time-frequency resource units (RUs). The possible use of RUs leads us to describe the considered frame structure.

In this article, we consider a total number of resources, U_{f_1} , dedicated to access preambles for the PRACH, as proposed in [9]. For the sake of clarity, we assume that the set of available preambles corresponds to the set of available subcarriers, U_{f_1} , as it happens for other cellular IoT technologies [36]. However, please note that the proposed model still applies for a general availability of preambles equal to U_{f_1} . The PRACH duration is denoted as τ_{prach} .

Then, the number of RUs available for UL transmissions depends on the configuration of the PUSCH and on its duration, denoted as τ_{pusch} . Given the RU slot interval equal to τ_{ru} , we denote the number of time slots in the PUSCH as $U_t = \frac{\tau_{pusch}}{\tau_{ru}}$. Conversely, U_{f_2} indicates the number of RUs available in the frequency domain of the PUSCH, where U_{f_2} is different from U_{f_1} in the general case. Overall, $U_t \cdot U_{f_2}$ are the RUs employed to uplink data transmission. We consider a single frame having length $\tau = \tau_{prach} + \tau_{pusch}$.

Therefore, depending on the value taken by U_{f_1} and U_{f_2} , it exists a certain probability that a node experiences a collision

TABLE I: General notations' description.

Notation	Description
\bar{n}	Mean number of nodes present in a cluster
\bar{n}_p	Mean number of parent points in the scenario
σ	TCP standard deviation for the nodes distribution
τ	Frame length
v	Speed of the UAB
h	Height of the UAB
U_{f_1}	Number of resources available for access preambles
U_{f_2}	Number of resources available for PUSCH in the frequency domain
U_t	Number of time slots in the PUSCH
p_c	Coverage probability
p_a	Access probability
p_b	Blocking probability
n_{att}	Number of possible access attempts for nodes during a UAB flight
\bar{p}_s	Mean success probability
\bar{S}_c	Mean cluster throughput
\bar{S}_n	Mean network throughput

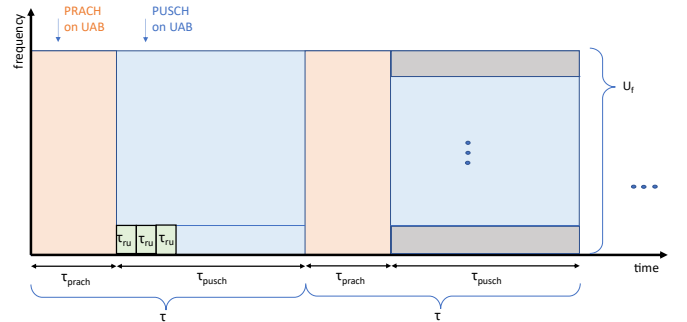


Fig. 3: A figurative example of time-frequency resources when two frames are considered on the time axis.

that denies its access in the PRACH and that it is blocked because of not sufficient RUs in the PUSCH, respectively. For mathematical tractability, we consider each node transmitting data in one subcarrier for the single frame duration. Also, though we consider frequency division duplex (FDD) mode for simplicity, the proposed model can be applied to both time division duplex (TDD) and FDD operations by modifying accordingly the timing of the throughput computation. Figure 3 represents an example of the frame structure. Then, the general notations used throughout the paper are defined in Table I.

V. STATIC SCENARIO WITH SINGLE ATTEMPT

This section reports the analysis and focuses only on the static case, where a single frame, τ , is considered and we assume each node has one data packet per τ to be transmitted; in case of no success in a single attempt, the data packet is considered as lost. Performance in terms of average cluster throughput, \bar{S}_c , equal to the sum of the achieved throughput

of nodes inside the same cluster, and average packet success probability, \bar{p}_s , are mathematically derived.

A. Notations

The following notations will be used:

- n_c : the number of nodes connected to the UAB;
- n_{aa} : the number of nodes that attempt to access the channel (i.e., attempt to have a successful transmission in the PRACH);
- n_{as} : the number of nodes that successfully access the channel (i.e., have a successful transmission in the PRACH);
- n_{af} : the number of nodes that fail in accessing the channel (i.e., no successful transmission in the PRACH);
- n_{rs} : the number of nodes that successfully get resources to be used in the PUSCH (i.e., have a successful transmission in the PUSCH);
- n_{rf} : the number of nodes that fail in getting resources to be used in the PUSCH (i.e., no successful transmission in the PUSCH).

As will be clarified later, all above random variables are distributed according to a PPP, with expected values, $\mathbb{E}\{\cdot\}$, hereafter denoted as \bar{n}_c , \bar{n}_{aa} , \bar{n}_{as} , \bar{n}_{af} , \bar{n}_{rs} , \bar{n}_{rf} , respectively (see below).

Other notations are:

- p_c : coverage probability, that is the probability that a node is covered by the UAB;
- p_a : access probability, that is the probability that a node successfully gets access to the channel;
- p_b : blocking probability, that is the probability that a node does not have RUs assigned in the PUSCH.

Finally, we indicate the Poissonian probability density function (pdf) as $\mathcal{P}(k, \bar{k}) = \frac{\bar{k}^k e^{-\bar{k}}}{k!}$.

B. Coverage Analysis

The coverage state determines if a node can reach and communicate with the UAB or if it is out of coverage. As an initial analysis, we start by studying the point-to-point coverage probability of one ground node inside a cluster to the UAB. Therefore, we consider a reference position for the UAB that coincides with the origin of our reference system at a constant height, h , $O = (0, 0, h)$. Then, being L_{thr} the threshold for the maximum loss, the probability that a node at distance d from O is covered by the UAB can be defined as:

$$p_c(d_{2D}) = \mathbb{P}\{L(d_{2D}, h) \leq L_{thr}\}. \quad (4)$$

Now, taking into account the LoS and NLoS components,

and the conditional probabilities definition, we have:

$$\begin{aligned} p_c(d_{2D}, h) &= p(d_{2D})\mathbb{P}\{L_1(d_{2D}, h) \leq L_{thr}\} \\ &\quad + (1-p(d_{2D}))\mathbb{P}\{L_n(d_{2D}, h) \leq L_{thr}\} \\ &= p(d_{2D}) \left[1 - \frac{1}{2} \operatorname{erfc} \left(\frac{L_{thr} - L_1^*}{2\sqrt{\sigma_{\xi_L}^2}} \right) \right] \\ &\quad + (1-p(d_{2D})) \left[1 - \frac{1}{2} \operatorname{erfc} \left(\frac{L_{thr} - L_n^*}{2\sqrt{\sigma_{\xi_n}^2}} \right) \right] \\ &= p(d_{2D})C_1(d_{2D}, h) + (1-p(d_{2D}))C_n(d_{2D}, h), \end{aligned} \quad (5)$$

$$C_1(d_{2D}, h) = \left[1 - \frac{1}{2} \operatorname{erfc} \left(\frac{L_{thr} - L_1^*}{2\sqrt{\sigma_{\xi_L}^2}} \right) \right], \quad (6a)$$

$$C_n(d_{2D}, h) = \left[1 - \frac{1}{2} \operatorname{erfc} \left(\frac{L_{thr} - L_n^*}{2\sqrt{\sigma_{\xi_n}^2}} \right) \right]. \quad (6b)$$

Then, given $f_{X,Y}(x, y) = \frac{1}{2\pi\sigma_x\sigma_y} e^{-\frac{x^2}{2\sigma_x^2}} e^{-\frac{y^2}{2\sigma_y^2}}$ and similarly to [11], we obtain the average coverage probability over one cluster when the UAV is placed at the origin as:

$$\bar{p}_c = \frac{1}{2\pi\sigma^2} \int_{-\infty}^{\infty} \int_{-\infty}^{\infty} p_c(\sqrt{x^2 + y^2}, h) e^{-\frac{x^2+y^2}{2\sigma^2}} dx dy. \quad (7)$$

Since each node is covered by the UAB with a constant average probability, \bar{p}_c , which is independent of the single node, the resulting process, n_c , is still Poissonian, with mean $\bar{n}_c = \bar{n} \cdot \bar{p}_c$, thanks to the thinning property of PPP [37]².

No approximations are introduced in the above formulation, so a perfect match between the mathematical model and simulations is expected (see Section VIII).

C. Channel Access and Blocking Probability

1) n_{aa} : In the CBRA approach, each node undergoes a random access procedure before being able to successfully obtain resources (i.e., grants) allocated to it in the PUSCH. According to the definition given above, this happens with a probability, p_a , that depends on the number of nodes attempting to access the channel, that is $n_{aa} = n_c$, and on the number of preambles available in the PRACH, U_{f_1} . Therefore, we have [36]³:

$$p_a(n_{aa}) = e^{-\frac{n_{aa}}{U_{f_1}}}. \quad (8)$$

Please note that in the case of CFRA it simply holds $p_a = 1$.

2) n_{as} : Since each node has success in the access with probability p_a , independent from node to node, the resulting process, n_{as} , is still Poissonian with mean $\bar{n}_{as} = \bar{n} \cdot \bar{p}_c \cdot \bar{p}_a$, thanks to the thinning property of PPP [37]⁴, where

$$\bar{p}_a = \sum_{n_{aa}=0}^{\infty} p_a(n_{aa}) \mathcal{P}(n_{aa}, \bar{n}_{aa}). \quad (9)$$

²This model can be applied also to other nodes distributions, provided that positions of nodes are still independent one each other.

³In case of finite population the analysis reported in [38] should be used as reference.

⁴This model can be applied also to other nodes distributions, provided that nodes are generating traffic in an independent way.

3) n_{rs} : Once a node is granted access to the channel, it needs to be scheduled RUs if they are available. If the number of resources available, U_{f_2} , is lower than the number of nodes requesting them, n_{as} , each node will suffer a blocking probability. Being n_{as} Poisson distributed with mean \bar{n}_{as} , we can use the Erlang-B formula for the blocking probability [39], given by⁵

$$p_b(\bar{n}_{as}) = \mathbf{B}(U_{f_2}, \bar{n}_{as}), \quad (10)$$

where the Erlang-B formula, $\mathbf{B}(\cdot)$, can be obtained in a recursive way as

$$\mathbf{B}(m, \bar{n}_{as}) = \frac{\bar{n}_{as} \mathbf{B}(m-1, \bar{n}_{as})}{m + \bar{n}_{as} \mathbf{B}(m-1, \bar{n}_{as})} \quad (11)$$

by setting $\mathbf{B}(0, \bar{n}_{as}) = 1$.

Therefore, n_{rs} is still Poisson distributed (same property as before), with mean $\bar{n}_{rs} = \bar{n} \cdot \bar{p}_c \cdot \bar{p}_a \cdot (1 - p_b(\bar{n}_{as}))$.

D. Performance Metrics

By recalling that a node can successfully transmit data if i) it is covered by the UAB; ii) it has success in accessing the channel; iii) it is not blocked (from the resource assignment viewpoint), the average cluster throughput in b/s is given by:

$$\begin{aligned} \bar{S}_c &= R \sum_{n=0}^{\infty} n \bar{p}_c p_a(n \bar{p}_c) (1 - p_b(\bar{n}_{as})) \mathcal{P}(n, \bar{n}) \\ &= R \sum_{n_{aa}=0}^{\infty} n_{aa} p_a(n_{aa}) (1 - p_b(\bar{n}_{as})) \mathcal{P}(n_{aa}, \bar{n}_{aa}), \quad (12) \end{aligned}$$

where R is the achievable rate for an IoT node that is covered by a static UAB and successfully receives the requested RUs, we set $R = M \frac{\tau_{pusch}}{\tau_{ru}} \frac{1}{\tau}$ [b/s], since in this case we assume a packet per frame can be generated. In Eq. (12) the cluster throughput is obtained by averaging over the statistics of n or, equivalently, of n_{aa} .

We can approximate the above formula as follows:

$$\bar{S}_c \cong R \bar{n}_{as} (1 - p_b(\bar{n}_{as})) = R \bar{n}_{rs}. \quad (13)$$

The comparison between simulations and mathematical model results will show the impact of the above approximation.

Finally, similarly to the average cluster throughput derivation, we can define the average packet success probability, \bar{p}_s :

$$\begin{aligned} \bar{p}_s &= \sum_{n=0}^{\infty} \bar{p}_c p_a(n \bar{p}_c) (1 - p_b(\bar{n}_{as})) \mathcal{P}(n, \bar{n}) \\ &= \sum_{n_{aa}=0}^{\infty} \bar{p}_c p_a(n_{aa}) (1 - p_b(\bar{n}_{as})) \mathcal{P}(n_{aa}, \bar{n}_{aa}) \\ &\cong \bar{p}_c p_a(\bar{n}_{aa}) (1 - p_b(\bar{n}_{as})). \quad (14) \end{aligned}$$

In Section VIII the mathematical model results are obtained by considering the approximated formula (last row of Eq. (14)). The comparison with simulations will show the impact of such an approximation.

⁵This formula can be applied to a generic traffic distribution [40].

VI. STATIC SCENARIO WITH MULTIPLE ATTEMPTS

Before moving to the dynamic scenario, we consider this intermediate case, allowing us to better clarify the differences between the static and the dynamic cases. Indeed, when considering the movement of the UAB, the following applies:

- the UAB is in coverage with nodes of a cluster for a given amount of time; therefore, nodes have different attempts to try to access the channel in the PRACH and to get resources in the PUSCH;
- the number of nodes covered by the UAB varies during the flight time.

Now, in order to study the impact of the two aspects above, at first separately and then jointly, in this section we just address the first aspect, while in the next section we account for both, providing a complete model for the dynamic case. Therefore, in this section, we still consider the UAB fixed in the center of the cluster, but we assume nodes have multiple attempts to try to access the channel and to get resources.

A. Notations

Since nodes can try to successfully transmit their data multiple times, we introduce the time variable. In particular, we assume the time axis is discretized in small intervals of duration τ , and we will denote as t the time steps. As a result, parameters defined in subsection V-A should be modified accounting for the time variable, t , that is: $n_c^{(t)}$, $n_{aa}^{(t)}$, $n_{as}^{(t)}$, $n_{af}^{(t)}$, $n_{rs}^{(t)}$, $n_{rf}^{(t)}$ and their expected values, $\bar{n}_c^{(t)}$, $\bar{n}_{aa}^{(t)}$, $\bar{n}_{as}^{(t)}$, $\bar{n}_{af}^{(t)}$, $\bar{n}_{rs}^{(t)}$, $\bar{n}_{rf}^{(t)}$. The other notations given in subsection V-A remain valid.

B. Coverage Analysis

Since we are still considering a static scenario, the coverage probability is the same derived in Section V. Therefore, we have that \bar{p}_c does not change by passing time and:

$$\bar{n}_c^{(t)} = \bar{n}_c = \bar{n} \bar{p}_c, \quad (15)$$

for all values of t .

C. Channel access and Blocking Probability

1) $n_{aa}^{(t)}$: As for the access to the channel is concerned, we must account for the following: i) nodes can try to access the channel more than once, so that at each attempt the number of nodes sending preambles and competing for RUs decreases; ii) if a node is blocked in a given attempt, (i.e., it successfully sends the request of resources, but these resources are not available), it can try to get resources at the following attempt (i.e., frame), without repeating the access procedure during the following PRACH. Therefore, the number of nodes trying to access the channel is equal to the number of nodes that are covered by the UAB at the first attempt, $t = 1$, and then it becomes the number of nodes that failed in accessing the channel at the previous attempts. We denote as n_{att} the number of attempts available to each node to try to transmit the data packet successfully⁶.

⁶While in this section this number is considered as a parameter, in the next one, it is mathematically derived, being the time the UAB is in connectivity with the cluster.

$$\begin{aligned}
S_c(n_{aa}^{(1)}, n_{aa}^{(2)}, \dots, n_{aa}^{(n_{att})}) &= R \sum_{t=1}^{n_{att}} S_c^{(t)} = R \left\{ n_{aa}^{(1)} p_a(n_{aa}^{(1)}) (1 - p_b(\bar{n}_{as}^{(1)})) \right. \\
&+ (1 - p_b(\bar{n}_{as}^{(2)})) [n_{aa}^{(1)} p_a(n_{aa}^{(1)}) p_b(\bar{n}_{as}^{(1)}) + n_{aa}^{(2)} p_a(n_{aa}^{(2)})] \\
&+ (1 - p_b(\bar{n}_{as}^{(3)})) [n_{aa}^{(1)} p_a(n_{aa}^{(1)}) p_b(\bar{n}_{as}^{(1)}) p_b(\bar{n}_{as}^{(2)}) + n_{aa}^{(2)} p_a(n_{aa}^{(2)}) p_b(\bar{n}_{as}^{(2)}) + n_{aa}^{(3)} p_a(n_{aa}^{(3)})] + \dots \left. \right\}. \quad (16)
\end{aligned}$$

Following the same approach used in Section V, it can be demonstrated that $n_{aa}^{(t)}$ is still Poisson distributed, with expected value:

$$\begin{aligned}
\bar{n}_{aa}^{(t)} &= \bar{n}_{af}^{(t-1)} = \bar{n}_{aa}^{(t-1)} (1 - p_a(\bar{n}_{aa}^{(t-1)})) \\
&= n_{aa}^{(1)} \prod_{m=1}^{t-1} (1 - p_a(n_{aa}^{(m)})), \quad (17)
\end{aligned}$$

with $\bar{n}_{aa}^{(1)} = \bar{n} \bar{p}_c$.

2) $n_{as}^{(t)}$: Being $n_{as}^{(t)}$ the number of nodes who successfully accessed the channel, at the current attempt or at the previous ones, and are now trying to get resources to transmit to the UAB, it is still Poisson distributed, with expected value:

$$\bar{n}_{as}^{(t)} = \bar{n}_{af}^{(t-1)} p_a(\bar{n}_{af}^{(t-1)}) + \bar{n}_{rf}^{(t-1)}, \quad (18)$$

where the first term is the average number of nodes who did not access the channel successfully in the previous $t-1$ attempts but has success in attempt t , and the second term is the average number of nodes who already managed to access the channel successfully, but did not find resources available in the previous attempt, $t-1$. $\bar{n}_{af}^{(t-1)}$ and $\bar{n}_{rf}^{(t-1)}$ can be derived iteratively by using the following formulas:

$$\begin{cases} \bar{n}_{af}^{(t-1)} &= \bar{n}_{aa}^{(t-1)} (1 - p_a(\bar{n}_{aa}^{(t-1)})) \\ \bar{n}_{rf}^{(t-1)} &= \bar{n}_{as}^{(t-1)} p_b(\bar{n}_{as}^{(t-1)}), \end{cases} \quad (19)$$

where $\bar{n}_{af}^{(t-1)}$ corresponds to nodes who failed in accessing the channel up to step $t-2$ and fail again in step $t-1$; while $\bar{n}_{rf}^{(t-1)}$ are nodes who failed in getting resources at $t-1$ (this happens with probability $p_b(\bar{n}_{as}^{(t-1)})$), even though they had success in accessing the channel before step $t-1$. Since the above formulas are obtained via an iterative procedure, initializing values are needed and they are set as follows:

$$\begin{cases} \bar{n}_{as}^{(1)} &= \bar{n}_{aa}^{(1)} p_a(\bar{n}_{aa}^{(1)}) \\ \bar{n}_{af}^{(1)} &= \bar{n}_{aa}^{(1)} (1 - p_a(\bar{n}_{aa}^{(1)})) \\ \bar{n}_{rf}^{(1)} &= \bar{n}_{as}^{(1)} p_b(\bar{n}_{as}^{(1)}). \end{cases} \quad (20)$$

3) $n_{rs}^{(t)}$: The number of nodes who are not blocked, $n_{rs}^{(t)}$, is still Poisson distributed with mean:

$$\bar{n}_{rs}^{(t)} = \bar{n}_{as}^{(t)} (1 - p_b(\bar{n}_{as}^{(t)})). \quad (21)$$

D. Performance Metrics

We now extend the formulation of the average cluster throughput proposed in Section V-D, to account for the multiple attempts, resulting in the sum of the throughput accumulated at each attempt. The latter is reported in Eq. (16),

where the average over the statistics of $n_{aa}^{(1)}, n_{aa}^{(2)}$, etc., still needs to be applied. The first term of Eq. (16) is the throughput obtained at the first attempt, which is the same as Eq. (12); the second term is the throughput obtained at the second attempt, where we have nodes who succeeded in accessing the channel at the first attempt but did not get resources, plus nodes who did not succeed in accessing the channel at the first attempt but succeed at the second one. The other terms are obtained following the same approach. R is the achievable rate for an IoT node that is covered by the UAB and successfully receives the requested RUs, that is: $R = M \frac{\tau_{pusch}}{\tau_{ru}} \frac{1}{n_{att} \tau}$ [b/s], since in this case we assume a packet every n_{att} frames is generated.

Now, by averaging over the statistics of $n_{aa}^{(1)}, n_{aa}^{(2)}$, etc. and generalizing, we obtain:

$$\begin{aligned}
\bar{S}_c &= R \sum_{t=1}^{n_{att}} \sum_{n_{aa}^{(t)}=0}^{\infty} \left\{ n_{aa}^{(t)} p_a(n_{aa}^{(t)}) \right. \\
&\cdot \left. \sum_{k=t}^{n_{att}} \left[(1 - p_b(\bar{n}_{as}^{(k)})) \prod_{l=t}^{k-1} p_b(\bar{n}_{as}^{(l)}) \right] \right\} \mathcal{P}(n_{aa}^{(t)}, \bar{n}_{aa}^{(t)}). \quad (22)
\end{aligned}$$

Similarly to the static case with a single attempt, we can define the approximated formula:

$$\bar{S}_c \cong R \sum_{t=1}^{n_{att}} \bar{n}_{as}^{(t)} (1 - p_b(\bar{n}_{as}^{(t)})) = R \sum_{t=1}^{n_{att}} \bar{n}_{rs}^{(t)}. \quad (23)$$

Finally, we can obtain the average packet success probability as follows:

$$\begin{aligned}
\bar{p}_s &= \sum_{t=1}^{n_{att}} \sum_{n_{aa}^{(t)}=0}^{\infty} \left\{ \bar{p}_c p_a(n_{aa}^{(t)}) \prod_{m=1}^{t-1} (1 - p_a(\bar{n}_{aa}^{(m)})) \right. \\
&\cdot \left. \sum_{k=t}^{n_{att}} \left[(1 - p_b(\bar{n}_{as}^{(k)})) \prod_{l=t}^{k-1} p_b(\bar{n}_{as}^{(l)}) \right] \right\} \mathcal{P}(n_{aa}^{(t)}, \bar{n}_{aa}^{(t)}) \\
&\cong \sum_{t=1}^{n_{att}} \left\{ \bar{p}_c p_a(\bar{n}_{aa}^{(t)}) \prod_{m=1}^{t-1} (1 - p_a(\bar{n}_{aa}^{(m)})) \right. \\
&\cdot \left. \sum_{k=t}^{n_{att}} \left[(1 - p_b(\bar{n}_{as}^{(k)})) \prod_{l=t}^{k-1} p_b(\bar{n}_{as}^{(l)}) \right] \right\}, \quad (24)
\end{aligned}$$

where we have used the following approximation for the sake of mathematical tractability:

$$n_{aa}^{(t)} \cong n_{aa}^{(1)} \prod_{m=1}^{t-1} (1 - p_a(\bar{n}_{aa}^{(m)})) = n \bar{p}_c \prod_{m=1}^{t-1} (1 - p_a(\bar{n}_{aa}^{(m)})). \quad (25)$$

Note that, when CFRA is considered, we can simply set $p_a = 1$.

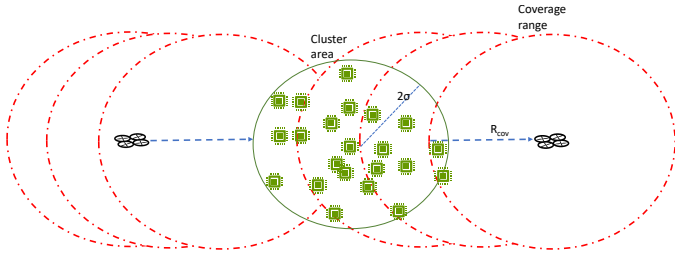


Fig. 4: Example of UAB crossing a cluster.

Finally, as in the case of the static scenario with a single attempt, approximated formulas will be used to show results, and the impact of the approximation is validated via comparison with simulations (see Section VIII).

VII. DYNAMIC SCENARIO

In this section, a fully dynamic model is considered. The implications of the UAB movement along the defined trajectory are the following:

- The number of nodes covered by the UAB at each step of its trajectory might change;
- The number of access attempts each device can make depends on the UAB position over time and the nodes' distribution inside the cluster (i.e., \bar{n} and σ).

The average network throughput, denoted as \bar{S}_n , gathered from the entire area (i.e., considering the different deployed clusters), is also derived in this case.

A. UAB Trajectory

For what concerns the UAB trajectory, we consider it follows a TSP solution over cluster centers flying at altitude h . The UAB only gradually gets in coverage with nodes in the cluster and it starts connecting with the first nodes before entering into the cluster circumference (i.e., at distances larger than 2σ), as shown in Fig. 4. In particular, coverage starts when the UAB is at a distance of 4σ from the cluster parent point; then, the UAB stays in coverage with the cluster nodes for a given amount of time, that is the time needed to cross the cluster area, denoted as τ_{cross} . By denoting as v the UAB speed, we have: $\tau_{\text{cross}} = \frac{8\sigma}{v}$, and the number of attempts during this time, that is the number of PRACH occurrences, is:

$$n_{\text{att}} = \frac{8\sigma}{v} \frac{1}{\tau}. \quad (26)$$

Fig. 4 gives an example of a UAB travelling on a straight line across a cluster and passing through the cluster parent point. Since the UAB follows the trajectory solution of a TSP, it will always cross the cluster center.

B. Coverage Analysis

We can now model the number of nodes covered by the UAB as those nodes present in the intersection region between the cluster area, \mathbf{A}_σ , and the UAB coverage area, \mathbf{A}_{cov} . As stated above, we approximate the UAB coverage area as a 2D circle with radius, $R_{\text{cov}} = 2\sigma$. This simplifies the analysis

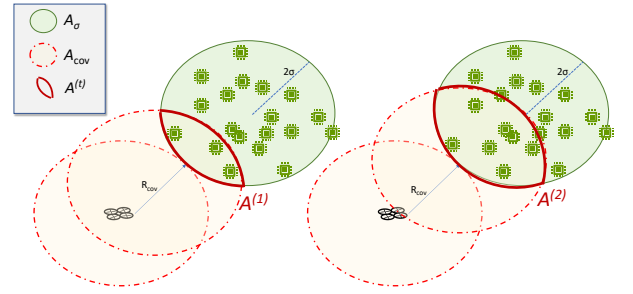


Fig. 5: Example of UAB approaching one cluster when $R_{\text{cov}} = 2\sigma$ and $n_{\text{att}} = 8$.

since now the two areas, \mathbf{A}_σ and \mathbf{A}_{cov} , are equal (see the example in Fig. 5). By passing time the UAB moves, and the intersection region changes by first increasing and then decreasing.

By denoting as $\mathbf{A}^{(t)}$, $t = 1, \dots, n_{\text{att}2}$ the area of intersection between the cluster area and the UAB coverage area (see Fig. 5), we can infer it as follows:

- Find the distance travelled by the UAB after step t as $d_{\text{uab}}^{(t)} = v \tau t$;
- Determine the distance of the UAB from the center of the cluster at step t , $d_{\text{cl}}^{(t)} = |4\sigma - d_{\text{uab}}^{(t)}|$, where $|\cdot|$ is the absolute value;
- Determine the area of intersection, $\mathbf{A}^{(t)}$, as:

$$y = \sqrt{(2\sigma)^2 - \left(\frac{d_{\text{cl}}^{(t)}}{2}\right)^2}$$

$$\mathbf{A}^{(t)} = 2(2\sigma)^2 \arcsin\left(\frac{y}{2\sigma}\right) - y d_{\text{cl}}^{(t)}. \quad (27)$$

At $t = 1$, the UAB is in coverage with nodes belonging to the intersection area $\mathbf{A}^{(1)}$ and, therefore, the number of nodes in coverage with the UAB and trying to access the channel is Poisson distributed with expected value: $\bar{n}_c^{(1)} = \bar{n}_{aa}^{(1)} = \bar{n} \bar{p}_c \frac{\mathbf{A}^{(1)}}{\mathbf{A}_\sigma}$. Later, from $t = 2$ to $t = \frac{n_{\text{att}2}}{2}$, the UAB covers new portions of the cluster area. Therefore, the nodes in coverage with the UAB are equal to those that were in coverage at the previous step, plus the new ones, that are included in the intersection area $\frac{|\mathbf{A}^{(2)} - \mathbf{A}^{(1)}|}{\mathbf{A}_\sigma}$.

Now, to derive the statistics of the number of nodes covered by the UAB when it goes out from the cluster, proper modelling of the entire TSP trajectory would be necessary, making the mathematical modelling extremely complex. However, since parent points of the TCP are deployed according to a PPP, the direction followed by the UAB to go out of the cluster is random (uniformly distributed in the 360 degrees on the 2D plane). To simplify the analysis we apply the following approximation. We consider the extreme cases: i) the UAB is assumed to travel over a straight line, on the 2D plane of the cluster (hereafter denoted as forward case, f); ii) once the UAB reaches the cluster center, it flies back from the cluster following the same flight segment (hereafter denoted as backward case, b). Then, performance is achieved by averaging among these two cases (b and f). Once again the comparison with simulations is used to check the impact of the approximation.

To generalize, we denote as $n_{ci}^{(t)}$ and $\bar{p}_{ci}^{(t)}$ the number of nodes connected in the intersection area at time step t and the corresponding mean connectivity probability, respectively. By considering $\mathbf{A}^{(0)} = 0$, it holds:

$$\bar{n}_{ci}^{(t)} = \bar{n} \bar{p}_c \left| \frac{\mathbf{A}^{(t)} - \mathbf{A}^{(t-1)}}{\mathbf{A}_\sigma} \right|, \text{ for } t = 2, \dots, n_{att}, \quad (28)$$

$$\bar{p}_{ci}^{(t)} = \bar{p}_c \left| \frac{\mathbf{A}^{(t)} - \mathbf{A}^{(t-1)}}{\mathbf{A}_\sigma} \right|, \text{ for } t = 2, \dots, n_{att}. \quad (29)$$

Then, we evince the total number of connected nodes at time step t , $\bar{n}_c^{(t)}$, and the resulting mean connectivity probability, $\bar{p}_c^{(t)}$:

$$\bar{n}_c^{(t)} = \begin{cases} \bar{n} \bar{p}_c \frac{\mathbf{A}^{(1)}}{\mathbf{A}_\sigma}, & \text{for } t = 1; \\ \sum_{a=1}^t \bar{n}_{ci}^{(a)}, & \text{for } t = 2, \dots, \frac{n_{att}}{2}; \\ \frac{1}{2} \sum_{a=t-(\frac{n_{att}}{2}-1)}^{\frac{n_{att}}{2}} \bar{n}_{ci}^{(a)} + \frac{1}{2} \sum_{a=1}^{n_{att}-t} \bar{n}_{ci}^{(a)}, & \\ \text{for } t = \frac{n_{att}}{2} + 1, \dots, n_{att} - 1; \end{cases} \quad (30)$$

$$\bar{p}_c^{(t)} = \begin{cases} \bar{p}_c \frac{\mathbf{A}^{(1)}}{\mathbf{A}_\sigma}, & \text{for } t = 1; \\ \sum_{a=1}^t \bar{p}_{ci}^{(a)}, & \text{for } t = 2, \dots, \frac{n_{att}}{2}; \\ \frac{1}{2} \sum_{a=t-(\frac{n_{att}}{2}-1)}^{\frac{n_{att}}{2}} \bar{p}_{ci}^{(a)} + \frac{1}{2} \sum_{a=1}^{n_{att}-t} \bar{p}_{ci}^{(a)}, & \\ \text{for } t = \frac{n_{att}}{2} + 1, \dots, n_{att} - 1; \end{cases} \quad (31)$$

where the first row refers to the initializing value, the second row is related to the increasing part, and the third one to the decreasing part, where the average between case f and b is applied. The expression can be explained as follows. For case f , the UAB is moving forward and the initially connected nodes will be the first to be out of coverage. For example, at $t = \frac{n_{att}}{2} + 1$, nodes seen at step $t = 1$ and belonging to $\mathbf{A}^{(1)}$ will no longer be able to connect and therefore, from this point on, they cannot attempt another time. On the opposite, in case b , the UAB moves backward and the set of nodes connected last will be the first to be out of coverage. For example, at $t = \frac{n_{att}}{2} + 1$, nodes getting connection at $t = \frac{n_{att}}{2}$ and belonging to $(\mathbf{A}^{(\frac{n_{att}}{2})} - \mathbf{A}^{(\frac{n_{att}}{2}-1)})$ cannot re-attempt access.

C. Channel Access and Blocking Probability

1) $n_{aa}^{(t)}$: As for the case of $\bar{n}_c^{(t)}$, in order to compute the average number of nodes attempting to access the channel at time step t , we need to take into account that for $t = 2, \dots, \frac{n_{att}}{2}$ at each step the number of nodes in coverage with the UAB increases, while for $t = \frac{n_{att}}{2} + 1, \dots, n_{att} - 1$, it starts decreasing. Therefore we have:

$$\bar{n}_{aa}^{(t)} = \begin{cases} \bar{n}_c^{(1)}, & \text{for } t = 1; \\ \sum_{a=1}^t \bar{n}_{ci}^{(a)} \prod_{l=a}^{t-1} (1 - p_a(\bar{n}_{aa}^{(l)})), & \text{for } t = 2, \dots, \frac{n_{att}}{2}; \\ \frac{1}{2} (\bar{n}_{aa,f}^{(t)} + \bar{n}_{aa,b}^{(t)}), & \text{for } t = \frac{n_{att}}{2} + 1, \dots, n_{att} - 1; \end{cases} \quad (32)$$

where, $\bar{n}_{aa,f}^{(t)}$ is given by:

$$\bar{n}_{aa,f}^{(t)} = \sum_{a=t-(\frac{n_{att}}{2}-1)}^{\frac{n_{att}}{2}} \bar{n}_{ci}^{(a)} \prod_{l=a}^{t-1} (1 - p_a(\bar{n}_{aa}^{(l)})), \quad (33)$$

$$\text{for } t = \frac{n_{att}}{2} + 1, \dots, n_{att} - 1,$$

and $\bar{n}_{aa,b}^{(t)}$ is given by:

$$\bar{n}_{aa,b}^{(t)} = \sum_{a=1}^{n_{att}-t} \bar{n}_{ci}^{(a)} \prod_{l=a}^{t-1} (1 - p_a(\bar{n}_{aa}^{(l)})), \quad (34)$$

$$\text{for } t = \frac{n_{att}}{2} + 1, \dots, n_{att} - 1.$$

2) $n_{as}^{(t)}$ and $n_{rs}^{(t)}$: As in the static case with multiple attempts, $n_{as}^{(t)}$ is Poisson distributed with expected value given by Eq. (18), where, however, $n_{aa}^{(t)}$ is given by Eq. (32) should be considered. The same holds for $n_{rs}^{(t)}$ still Poisson distributed with expected value, given by Eq. (21), where, however $n_{aa}^{(t)}$ given by Eq. (32) should be considered.

D. Performance Metrics

To derive the average cluster throughput we can reuse the same formulation presented for the static case with multiple attempts, that is Eq. (23) and substitute $n_{aa}^{(t)}$ with Eq. (32).

As far as the average packet success probability is concerned, we followed a similar approach, but we report here also the final formula due to its complexity. In particular, the metric is obtained as the sum of the average success probability obtained at each attempt, that is:

$$\bar{p}_s = \sum_{t=1}^{n_{att}} \bar{p}_s^{(t)}, \quad (35)$$

where $\bar{p}_s^{(t)}$ is given by (for the sake of conciseness we report directly the approximated formula used in Section VIII):

$$\bar{p}_s^{(t)} \cong \begin{cases} \bar{p}_c^{(1)} p_a(\bar{n}_{aa}^{(1)}) (1 - p_b(\bar{n}_{as}^{(1)})), & \text{for } t = 1; \\ (1 - p_b(\bar{n}_{as}^{(t)})) \left[\sum_{a=1}^t p_a(\bar{n}_{aa}^{(a)}) \prod_{k=a}^{t-1} p_b(\bar{n}_{as}^{(k)}) \right. \\ \left. \left(\sum_{l=1}^a \bar{p}_{ci}^{(l)} \prod_{m=l}^{a-1} (1 - p_a(\bar{n}_{aa}^{(m)})) \right) \right], & \text{for } t = 2, \dots, \frac{n_{att}}{2}; \\ \frac{1}{2} (\bar{p}_{s,f}^{(t)} + \bar{p}_{s,b}^{(t)}), & \text{for } t = \frac{n_{att}}{2} + 1, \dots, n_{att} - 1; \end{cases} \quad (36)$$

where

$$\bar{p}_{s,f}^{(t)} = (1 - p_b(\bar{n}_{as}^{(t)})) \left[\sum_{a=t-(\frac{n_{att}}{2}-1)}^{\frac{n_{att}}{2}} p_a(\bar{n}_{aa}^{(a)}) \prod_{k=a}^{t-1} p_b(\bar{n}_{as}^{(k)}) \right. \\ \left. \cdot \sum_{l=1}^a \bar{p}_{ci}^{(l)} \prod_{m=l}^{a-1} (1 - p_a(\bar{n}_{aa}^{(m)})) \right], \quad (37)$$

$$\text{for } t = \frac{n_{att}}{2} + 1, \dots, n_{att} - 1,$$

TABLE II: Network and Channel Parameters.

Parameter	Notation	Value
Square area side	Q	10 km
Parent point density	λ_p	0.05 [km^{-2}]
Maximum loss threshold	L_{thr}	112 dB
Carrier frequency	f_c	27.5 GHz
RU duration	τ_{ru}	0.25 ms
PRACH duration	τ_{prach}	1 ms

$$\bar{p}_{s,b}^{(t)} = (1 - p_b(\bar{n}_{as}^{(t)})) \left[\sum_{a=1}^{n_{\text{att}}-t} p_a(\bar{n}_{aa}^{(a)}) \prod_{k=a}^{t-1} p_b(\bar{n}_{as}^{(k)}) \right. \\ \left. \cdot \sum_{l=1}^a \bar{p}_{ci}^{(l)} \prod_{m=l}^{a-1} (1 - p_a(\bar{n}_{aa}^{(m)})) \right], \\ \text{for } t = \frac{n_{\text{att}}}{2} + 1, \dots, n_{\text{att}} - 1. \quad (38)$$

Finally, we can infer the average throughput of the overall network, \bar{S}_n , by summing the ones achieved from present clusters:

$$\bar{S}_n = \sum_{n_p=0}^{\infty} n_p \bar{S}_c \mathcal{P}(n_p, \bar{n}_p) \quad (39)$$

where we remind that n_p follows a PPP with mean \bar{n}_p . Note that in this case, since we are accounting for the entire flight, R is set equal to $R = M \frac{\tau_{\text{pusch}}}{\tau_{\text{ru}}} \frac{1}{\tau_{\text{fly}}}$ [b/s], where τ_{fly} is the time needed to perform the entire TSP.

VIII. NUMERICAL RESULTS

The proposed model is now compared to simulations to prove the impact of the introduced approximations. As anticipated, the software used for simulations was built on purpose and is available at [15]. To be more specific on the major details, i) shadowing samples for connectivity are extracted randomly each time for each node as per the loss distribution in Sec. III.B; ii) the access preambles are sampled randomly and uniformly and compared to each other checking if nodes select the same preamble and thus their packets collide; iii) time and space are discretized to simulate the UAB trajectory and update the UAB position in the dynamic case; iv) the TSP is solved using dynamic programming [41]. To achieve appropriate statistics, we run 10^4 samples from Monte-Carlo simulations, and then evaluate our system model with parameters set as shown in Table II. Other default values are set as the following: $h = 100$ m, $\sigma = 10$ m, $v = 30$ m/s, $M = 28$, $\tau = 126$ ms, if not specified otherwise. We first analyze the nodes' coverage probability for the static and dynamic cases, and then we move to the performance in terms of \bar{p}_s and \bar{S}_c .

A. Coverage Analysis

Fig. 6 reports \bar{p}_c for the static case, as a function of σ , when varying h . We can observe as the curves show the same decreasing trend: \bar{p}_c decreases with σ , because nodes are scattered in an area (the cluster area) whose radius is 2σ ; while it increases by getting h lower, due to shorter distances. As expected, the comparison between the mathematical model and

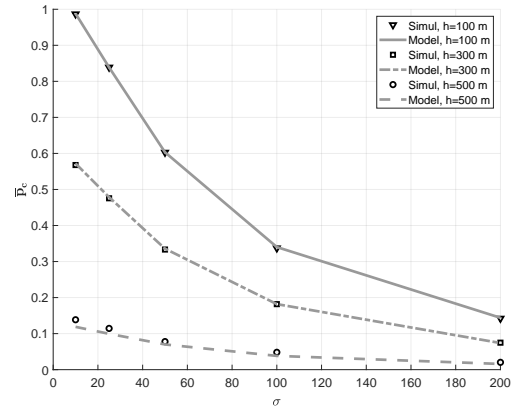


Fig. 6: Coverage probability for the static case, when varying σ and h .

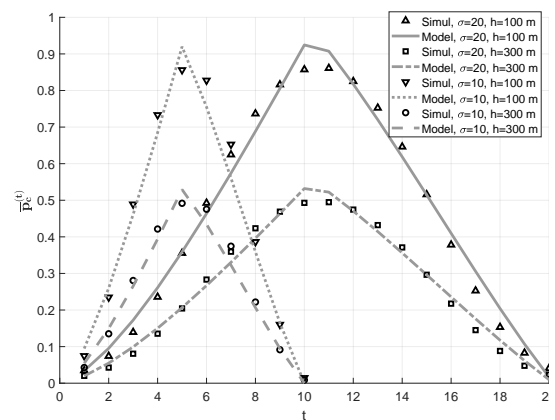


Fig. 7: Coverage probability for the dynamic case, as a function of time, t , by varying σ and h .

simulation results shows a perfect match (no approximations introduced).

The coverage probability changes when considering a fully dynamic scenario. Results, in terms of $\bar{p}_c^{(t)}$ as a function of time, t , by varying σ and h , are reported in Fig. 7.

Once again mathematical model and simulation results are reported. Note that changing σ means varying also the length of the path travelled by the UAB over the cluster area; thus, n_{att} is modified accordingly (in Fig. 7 we have $n_{\text{att}} = [10, 20]$ corresponding to $\sigma = [10, 20]$, respectively). Though the fitting between the model and simulations is not perfect, we can observe that the assumptions made (see Section VII-B) do not affect significantly the results. Indeed, by focusing for example on the curve having $\sigma = 20$ and $h = 100$ m, the model i) captures the increasing trend of $\bar{p}_c(t)$ while the UAB approaches the cluster center, ii) presents a maximum when the UAB reaches the cluster center, and iii) has a decreasing trend when the UAB starts moving away from the cluster center. Furthermore, note that by increasing σ (i.e., n_{att}) the maxima are reached later since it takes more time for the UAB to reach the cluster center. Finally, the maxima reached in curves of Fig. 7 never go above the static value of \bar{p}_c in Fig. 6, as

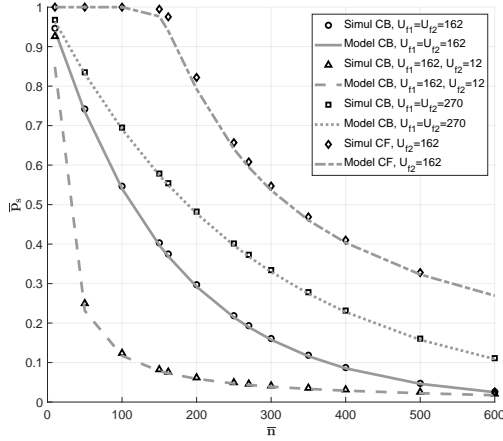


Fig. 8: Average success probability for the static scenario with single attempt.

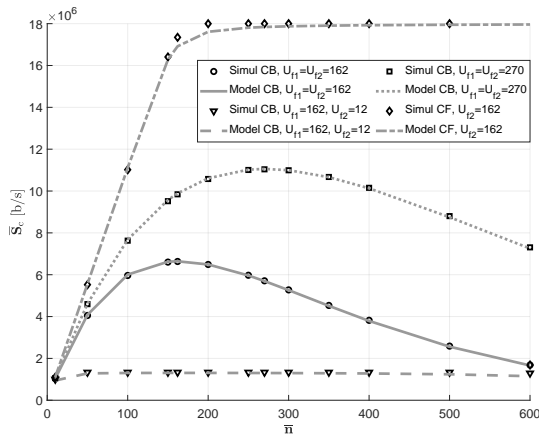


Fig. 9: Average cluster throughput for the static scenario with single attempt.

expected.

B. Static Scenario With Single Attempt

The average success probability, \bar{p}_s , is shown in Fig. 8, while varying the mean number of nodes per cluster, \bar{n} . Similarly, the average cluster throughput, \bar{S}_c , is shown over \bar{n} in Fig. 9. In both plots, modelling and simulations present different cases: i) CF access where only the blocking probability has impact, ii) CB access where only the access probability has impact (i.e., $U_{f1} = U_{f2} = 162$ and $U_{f1} = U_{f2} = 270$), and iii) CB access with $U_{f1} = 162$, $U_{f2} = 12$, where both access and blocking probabilities take effect.

\bar{p}_s decreases when increasing \bar{n} (i.e., the traffic load) since the number of preambles and uplink resources is limited. In particular, case i) with CF shows a higher \bar{p}_s as compared to the other cases, because nodes are not limited by the access contention. The success probability starts decreasing when \bar{n} becomes larger than U_{f2} . This also shows that possible preamble collisions have a higher impact than blocking occasions in this case. However, curves of case ii) show clearly that with a higher number of different preambles given by U_{f1} ,

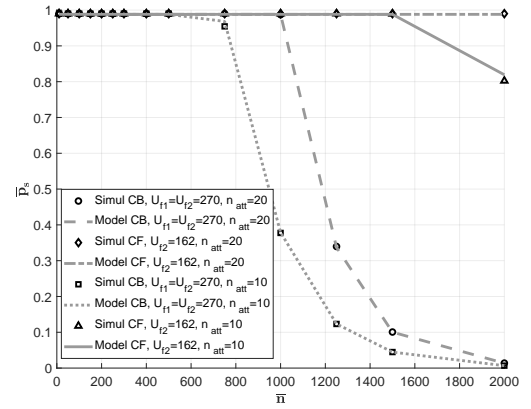


Fig. 10: Average success probability as a function of \bar{n} for the static scenario with multiple attempts.

the access probability gets higher, consequently increasing the success probability. Finally, in case iii), nodes undergo both contentions in the access procedure and blocking because of a small number of resources available ($U_{f2} = 12$), and therefore the success probability becomes lower.

As far as the throughput is concerned, we can notice the following: in case i), \bar{S}_c grows with \bar{n} until resources U_{f2} are available; then, at $\bar{n} = U_{f2}$, the curve stops increasing linearly and reaches an upper bound; in the two curves of case ii) \bar{S}_c reaches two maxima for different values of \bar{n} ; indeed, when \bar{n} is low, the system is limited by coverage, while, when $\bar{n} > \frac{U_{f1}}{p_c}$, the number of collisions increases and the system becomes limited by the access contention. These maxima can be mathematically derived by setting $\frac{d\bar{S}_c}{d\bar{n}} = 0$, from which we infer for the CB case with $p_b = 0$: $\bar{n}_{opt} = \frac{U_{f1}}{p_c}$, and the optimum average cluster throughput: $\bar{S}_{c,opt} = R U_{f1} / e$. Finally, the last curve presents smaller throughput values, due to the lower \bar{p}_s , as discussed previously.

In all cases above we can observe a good match between the model and simulations, demonstrating a slight impact of the introduced approximations.

C. Static Scenario With Multiple Attempts

Figs. 10 and 11 show \bar{p}_s and \bar{S}_c when $n_{att} = [10, 20]$, considering both CF and CB curves from the cases analysed before.

Similar trends to the previous section can be observed; however, larger values of \bar{p}_s (as compared to those reported in Fig. 8) are shown. This is because nodes have multiple trials to try to get access to the channel and may wait for resources a number of n_{att} attempts. Clearly, as the value of n_{att} increases, the success probability increases and curves shift to the right.

Fig. 11 shows the throughput metric for the same set of curves of Fig. 10. Let us focus on curves with CF access first. The CF curve with $n_{att} = 10$ presents an upper bound (similar to the static scenario with a single attempt) for $\bar{n} > 2000$. On the contrary, when n_{att} increases to 20, the upper bound is not present since this higher number of attempts allows to

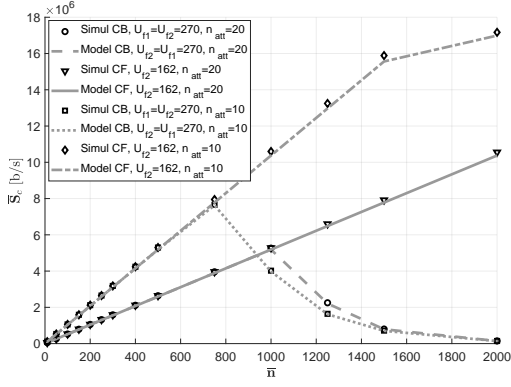


Fig. 11: Average cluster throughput as a function of \bar{n} for the static scenario with multiple attempts.

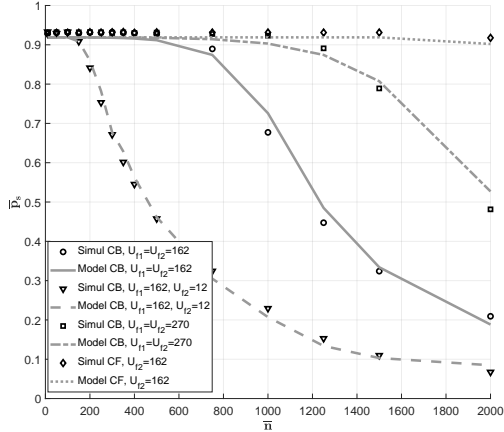


Fig. 12: Average success probability for the dynamic case when setting $\tau_{pusch} = 125$ ms and $n_{att} = 20$.

reach $\bar{p}_s = 1$. Similarly to the results shown in the previous section, the CB curves show a maximum: for low values of \bar{n} the scenario is limited by connectivity and traffic demand, while when \bar{n} is high it is limited by access and requests overload. As n_{att} increases, the optimum number of nodes per cluster increases too, thanks to the higher number of trials for transmitting the UL data. Interestingly, for smaller values of \bar{n} , all curves show a linear increase, with a deterministic slope. Indeed, when \bar{n} is small, \bar{p}_s is almost one, and therefore, $\bar{S}_c \simeq \bar{n} R$. Please note that throughput absolute values are not comparable with those of the static scenario with a single attempt, since in the multi-attempt scenario each node has to transmit a data packet every $\tau \cdot n_{att}$ frames, rather than every τ . Again, all curves obtained with the proposed mathematical modelling present a good match with simulations.

D. Dynamic Scenario

We now analyze the dynamic scenario, with the aim of checking the approximations introduced. Figures 12 and 13 show \bar{p}_s and \bar{S}_c , respectively, when $\tau = 126$ ms. For consistency with previous results, the same set of curves and cases from i) to iii) is shown in both figures. By focusing first on Fig. 13, one can observe the impact of the approximation

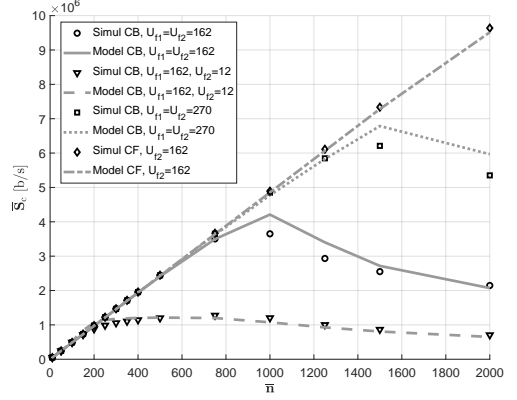


Fig. 13: Average cluster throughput for the dynamic case when setting $\tau_{pusch} = 125$ ms and $n_{att} = 20$.

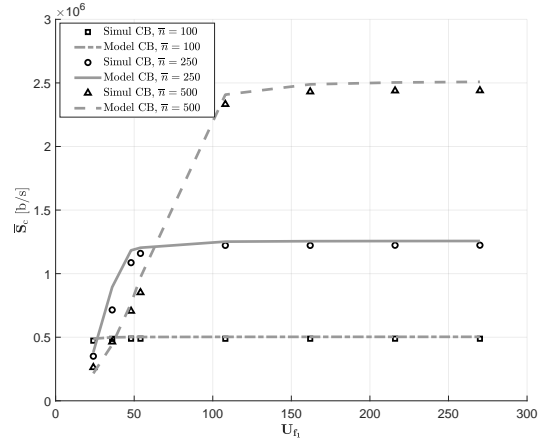


Fig. 14: Average cluster throughput for the dynamic case when varying U_{f1} , $\tau_{pusch} = 125$ ms and $n_{att} = 20$.

made on the modelling of the trajectory. However, given the level of simplification of a potentially too complex problem to be solved in closed formulas, the gap is not significant. Indeed, the model captures the metric main trend for the different possible combinations of access type and uplink resources. When comparing \bar{p}_s values with those reported for the static multi-attempt scenario, a general improvement of the performance can be observed. This happens because nodes get connected only *gradually* following Eq. (30) and not all of the \bar{n} nodes attempt to access at the same time, i.e. the access probability (Eq. (8)) has a smaller numerator at the exponent and increases. A slow UAB approaching the cluster results as a sort of *barring* technique [8] to avoid the overloading of access requests.

As far as the average cluster throughput is concerned, curves of Fig. 13 show a similar trend w.r.t. those reported in Fig. 11; however, a notable improvement can be observed in case ii): the maximum is reached for a higher value of \bar{n} and the resulting \bar{S}_c is much larger. This reflects what was observed previously for \bar{p}_s , and the barring effect improving the access contention.

For a better insight into the UAB parameters' impact, we discuss the effects of U_{f1} and v .

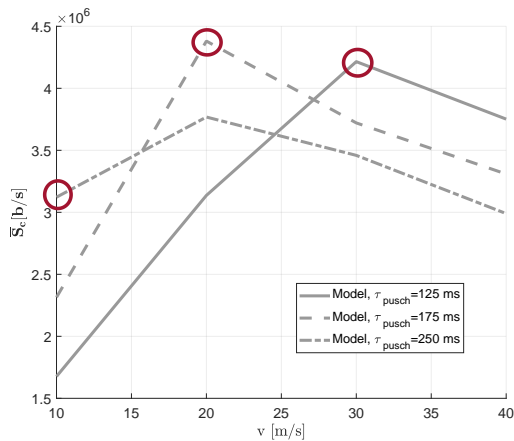


Fig. 15: Average cluster throughput for the dynamic case when varying v and τ_{pusch} ; $\bar{n} = 1000$.

Fig. 14 shows \bar{S}_c , while varying the number of available preambles, U_{f_1} . Clearly, this impacts only the CB case, and therefore no curves for CF access are shown. These curves also present a good match of the model with simulations. If we focus first on the upper curve, when $\bar{n} = 500$, we notice an initial increase until a bound is reached. Given the large number of attempts, $n_{att} = 20$, a number of preambles $U_{f_1} = 150$ suffices to serve all $\bar{n} = 500$ nodes. The other two curves have a similar trend. This suggests that dedicating a larger number of resources to preambles results in a waste of resources. Therefore, the model is proved to be efficient in helping operators properly set design parameters. Another interesting behaviour is the following; when the number of nodes contending is smaller (e.g., $\bar{n} = 250$), the U_{f_1} value to reach the bound lowers, and the value of \bar{S}_c is inevitably larger than the case in which the contending \bar{n} increases.

Figure 15 shows the trend of \bar{S}_c , as a function of v , for different values of τ_{pusch} . To properly understand the plot, please note that both v and τ_{pusch} impact on n_{att} (see Eq. (26)) and on R . In particular, by increasing v (having fixed τ_{pusch}), or τ_{pusch} (having fixed v), on one hand, n_{att} gets lower, resulting in lower throughput, but, on the other hand, we also have an increase of R . When the trade-off between these two effects is found, there exist optima. Also note that the optimum value of τ_{pusch} varies with v and, in particular, it decreases with v . This is because, for low values of v , the impact of an increasing R with τ_{pusch} is stronger than the decreasing of n_{att} , therefore larger values of τ_{pusch} are better; then, a large value of v impacts more the decreasing of n_{att} , resulting in a maximum for lower values of τ_{pusch} (see the red points in the figure). Finally, note that the existence of an optimum value of τ_{pusch} means that there exists an optimal number of resources to be used for the PUSCH (i.e., U_t).

Another fundamental aspect that we can evince from this work is the comparison of results when considering a UAB flying over the cluster of IoT nodes (i.e., dynamic scenario), and the case where the UAB is hovering above one cluster (i.e., static scenario). By considering the same time window for the two cases, that is the interval of time during which the UAB is in connectivity with the IoT nodes of the cluster, in Fig. 16 we

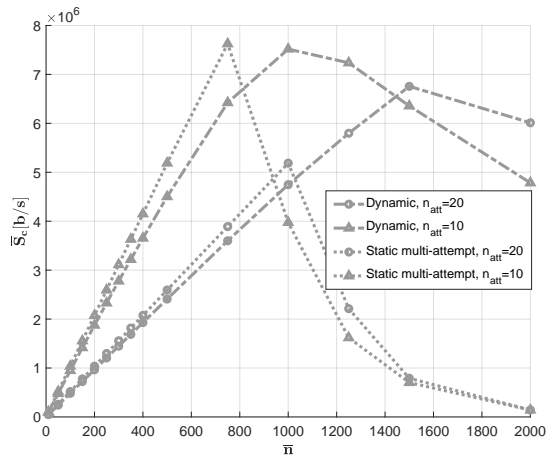


Fig. 16: Dynamic versus Static multi-attempt modelling for the CB case when $U_{f_1} = U_{f_2} = 270$.

TABLE III: Cluster throughput: comparing one-hop and two-hop communication strategies.

\bar{n}	S_c [kb/s]			
	500	1000	1500	2000
One-Hop Communication	2409	4747	6757	6012
Two-Hop Communication via CHs	2625	5249	740	132

plot the cluster throughput, \bar{S}_c , while varying \bar{n} when setting $n_{att} = 10$ and $n_{att} = 20$. We consider the case of CB access with a resource availability of $U_{f_1} = U_{f_2} = 270$. Clearly, since the time window considered is longer than a frame, the static scenario is with multiple attempts (see Sec. VI). As previously explained for the curves with $n_{att} = 20$, all plots present a maximum in correspondence of a certain \bar{n} . If we focus on the curves with $n_{att} = 20$, we can observe that the throughput of the dynamic and static scenarios increases linearly, with almost the same slope. However, the static scenario reaches its maximum at $\bar{n} = 1000$, while the dynamic one continues to increase until $\bar{n} = 1500$. This reflects what was observed for \bar{p}_s since after these points \bar{p}_s started to decrease. Therefore, in general, a moving UAB can serve a higher number of nodes. The curves with $n_{att} = 10$ show similar behavior. Since in these curves the time window is smaller, the throughput is higher but fewer nodes than the case with $n_{att} = 20$ are covered. Furthermore, please note that both the curves of the static scenario have a sharp decrease after the maximum, while the curves of the dynamic scenario have a more gentle descent. This suggests that for a high number of nodes per cluster, the movement of the UAB notably improves the performance, while, when few nodes are present, the performance is similar (there is a slight improvement for the static case, because of the Gaussian distribution of IoT nodes in the cluster, resulting in a larger density of nodes around the parent point, where the UAB in a static position is located).

As an additional comparison, we might evaluate the achievable performance, obtained through a one-hop communication strategy, where IoT directly transmit to the UABS, with respect

TABLE IV: Network Throughput Results.

\bar{n}_p	S_n [kb/s]			
	2	4	6	8
$v = 20$ m/s	70.06	108.03	134.21	156.89
$v = 30$ m/s	94.15	145.19	180.37	210.85
$v = 40$ m/s	83.8	129.22	160.54	187.67

to a two-hop strategy, where IoT nodes first transmit their data packets to a central node located at the nearby parent point, and then this node sends the collected data to the UAB. This lets a possible grid-powered node handle the access procedure. By assuming the same protocol is employed, we might compare this strategy with our dynamic modelling described in Sec. VII. To model the different strategies, we focus on the first hop, which is the link between the IoT nodes of the cluster with the parent point, a node we will refer to as the cluster head (CH). Here, the mean connectivity probability, \bar{p}_c , changes and has to be recomputed depending on the CH height, h_c , which is equal to the other nodes' height, $h_u = 1.5$ m. Since the protocol remains the same, the access probability, p_a , is described in Eq. (8), the blocking probability, p_b , in Eq. (10) and the cluster throughput, \bar{S}_c in Eq. (23). Then, we consider the UAB able to fly exactly above each CH to receive all the collected data; to simplify this approach, we assume that the link between the CH and the UAB (that is the second hop) is robust, i.e., $\bar{p}_c = 1$, and then $\bar{p}_a = 1$ and $\bar{p}_b = 0$. Further, we may assume that protocol delays in the same link are negligible and thus focus on the link between the IoT nodes and the CH. Numerical results are described in Table III. As one might notice, the comparison between these strategies resembles the comparison of the static with multiple attempts and dynamic scenarios, thus having our dynamic protocol performing better for large values of \bar{n} .

To conclude the numerical analysis, we evaluate the network throughput, \bar{S}_n , while varying the mean number of parent points, \bar{n}_p . With this computation, we need to account for the whole TSP trajectory over the entire area with side Q . Table IV shows numerical values with different UAB's speeds, v . When the speed v increases, we observe the behaviour already discussed in Fig. 15. Moreover, as expected, by increasing \bar{n}_p , and therefore the average number of nodes present in the area, the overall network throughput increases.

IX. CONCLUSIONS

In this article, we provide an insightful mathematical analysis of a UAB-aided network for clustered RedCap UEs. The model incorporates the UE-UAB coverage analysis at mm-Wave, considering both static and dynamic scenarios, contention-based and contention-free access approaches, and blocking events due to the possible unavailability of UL resources. The average success probability and throughput are derived mathematically, and the comparison with Monte-Carlo simulations shows a good correspondence.

The model allows obtaining the optimum number of nodes per cluster and the optimum speed of the UAB, maximizing the throughput. Further, the model reveals an effective design of

access and uplink resources (i.e., PRACH and PUSCH), given the number of possible multiple attempts. While the PUSCH should accommodate enough resources to avoid blocking events, there exists an optimal trade-off between the number of PRACH occurrences, the UAB speed, and the duration of the PUSCH to enhance the achievable throughput.

ACKNOWLEDGMENT

This work has been carried out in the framework of the CNIT National Laboratory WiLab and the WiLab-Huawei Joint Innovation Center. We would like to thank Aman Jassal for the very fruitful discussion on this paper.

REFERENCES

- [1] Y. Zeng, Q. Wu, and R. Zhang, "Accessing From the Sky: A Tutorial on UAV Communications for 5G and Beyond," *Proceedings of the IEEE*, vol. 107, no. 12, pp. 2327–2375, 2019.
- [2] M. Mozaffari *et al.*, "A tutorial on UAVs for wireless networks: Applications, challenges, and open problems," *IEEE communications surveys & tutorials*, vol. 21, no. 3, pp. 2334–2360, 2019.
- [3] G. Geraci *et al.*, "What Will the Future of UAV Cellular Communications Be? A Flight from 5G to 6G," *IEEE Communications Surveys & Tutorials*, pp. 1–1, 2022.
- [4] F. Qi *et al.*, "UAV Network and IoT in the Sky for Future Smart Cities," *IEEE Network*, vol. 33, no. 2, pp. 96–101, 2019.
- [5] R. Verdona and S. Mignardi, "Joint aerial-terrestrial resource management in UAV-aided mobile radio networks," *IEEE Network*, vol. 32, no. 5, pp. 70–75, 2018.
- [6] N. Xia, H.-H. Chen, and C.-S. Yang, "Radio resource management in machine-to-machine communications—a survey," *IEEE Communications Surveys & Tutorials*, vol. 20, no. 1, pp. 791–828, 2017.
- [7] N. Xia, H.-H. Chen, and C.-s. Yang, "Emerging technologies for machine-type communication networks," *IEEE Network*, vol. 34, no. 1, pp. 214–222, 2019.
- [8] H. S. Jang *et al.*, "Resource-Optimized Recursive Access Class Barring for Bursty Traffic in Cellular IoT Networks," *IEEE Internet of Things Journal*, vol. 8, no. 14, pp. 11 640–11 654, 2021.
- [9] H. S. Jang *et al.*, "Resource-Hopping-Based Grant-Free Multiple Access for 6G-Enabled Massive IoT Networks," *IEEE Internet of Things Journal*, vol. 8, no. 20, pp. 15 349–15 360, 2021.
- [10] J. Liu *et al.*, "Online control of preamble groups with priority in massive IoT networks," *IEEE Journal on Selected Areas in Communications*, vol. 39, no. 3, pp. 700–713, 2020.
- [11] S. Mignardi and C. Buratti, "On the modelling of UAV-Aided NB-IoT Networks," *IEEE Global Communications Conference (GLOBECOM)*, 2021.
- [12] S. Mignardi *et al.*, "Unmanned aerial base stations for NB-IoT: Trajectory design and performance analysis," in *2020 IEEE 31st Annual International Symposium on Personal, Indoor and Mobile Radio Communications*. IEEE, 2020, pp. 1–6.
- [13] "Support of reduced capability NR devices," *3GPP RP 202933 version*, Dec. 2020.
- [14] O. M. Bushnaq, A. Chaaban, and T. Y. Al-Naffouri, "The Role of UAV-IoT Networks in Future Wildfire Detection," *IEEE Internet of Things Journal*, vol. 8, no. 23, pp. 16 984–16 999, 2021.
- [15] "Open UAB-IoT simulator software." [Online]. Available: <https://www.unibo.it/sitoweb/c.buratti/useful-contents>
- [16] S. Yan, M. Peng, and X. Cao, "A Game Theory Approach for Joint Access Selection and Resource Allocation in UAV Assisted IoT Communication Networks," *IEEE Internet of Things Journal*, vol. 6, no. 2, pp. 1663–1674, 2019.
- [17] N. H. Motlagh, M. Bagaa, and T. Taleb, "Energy and Delay Aware Task Assignment Mechanism for UAV-Based IoT Platform," *IEEE Internet of Things Journal*, vol. 6, no. 4, pp. 6523–6536, 2019.
- [18] Y. Liu *et al.*, "Resource Allocation and 3-D Placement for UAV-Enabled Energy-Efficient IoT Communications," *IEEE Internet of Things Journal*, vol. 8, no. 3, pp. 1322–1333, 2021.
- [19] N. Nacementouri *et al.*, "Three-Dimensional Multi-UAV Placement and Resource Allocation for Energy-Efficient IoT Communication," *IEEE Internet of Things Journal*, vol. 9, no. 3, pp. 2134–2152, 2022.

- [20] H. Yan *et al.*, “Data Offloading Enabled by Heterogeneous UAVs for IoT Applications under Uncertain Environments,” *IEEE Internet of Things Journal*, pp. 1–1, 2022.
- [21] B. Galkin, J. Kibilda, and L. A. DaSilva, “Coverage Analysis for Low-Altitude UAV Networks in Urban Environments,” in *GLOBECOM 2017 - 2017 IEEE Global Communications Conference*, 2017, pp. 1–6.
- [22] V. V. Chetlur and H. S. Dhillon, “Downlink Coverage Analysis for a Finite 3-D Wireless Network of Unmanned Aerial Vehicles,” *IEEE Transactions on Communications*, vol. 65, no. 10, pp. 4543–4558, 2017.
- [23] X. Zhou *et al.*, “Underlay Drone Cell for Temporary Events: Impact of Drone Height and Aerial Channel Environments,” *IEEE Internet of Things Journal*, vol. 6, no. 2, pp. 1704–1718, 2019.
- [24] F. Linsalata, M. Magarini, and U. Spagnolini, “Stochastic Modelling of LoS Aggregate Interference in Uplink of Aerial Base Station-assisted Network,” in *2021 IEEE Globecom Workshops (GC Wkshps)*, 2021, pp. 1–6.
- [25] S. Zhang, J. Liu, and W. Sun, “Stochastic Geometric Analysis of Multiple Unmanned Aerial Vehicle-Assisted Communications Over Internet of Things,” *IEEE Internet of Things Journal*, vol. 6, no. 3, pp. 5446–5460, 2019.
- [26] C.-S. Choi, F. Baccelli, and G. d. Veciana, “Modeling and Analysis of Data Harvesting Architecture Based on Unmanned Aerial Vehicles,” *IEEE Transactions on Wireless Communications*, vol. 19, no. 3, pp. 1825–1838, 2020.
- [27] B. Li *et al.*, “Performance Analysis and Optimization for the MAC Protocol in UAV-Based IoT Network,” *IEEE Transactions on Vehicular Technology*, vol. 69, no. 8, pp. 8925–8937, 2020.
- [28] A. Mahmoud *et al.*, “Intelligent Reflecting Surfaces Assisted UAV Communications for IoT Networks: Performance Analysis,” *IEEE Transactions on Green Communications and Networking*, vol. 5, no. 3, pp. 1029–1040, 2021.
- [29] R. Han *et al.*, “Age of Information and Performance Analysis for UAV-Aided IoT Systems,” *IEEE Internet of Things Journal*, vol. 8, no. 19, pp. 14447–14457, 2021.
- [30] M. Haenggi, *Stochastic Geometry for Wireless Networks*. U.K.: Cambridge Univ. Press, 2012.
- [31] “Technical Specification Group Radio Access Network; Study on channel model for frequencies from 0.5 to 100 GHz,” *3GPP TR 38.901 version 16.1.0*, Dec. 2019.
- [32] Q. M. Ha *et al.*, “On the min-cost traveling salesman problem with drone,” *Transportation Research Part C: Emerging Technologies*, vol. 86, pp. 597–621, 2018.
- [33] R. Abozariba *et al.*, “NOMA-Based Resource Allocation and Mobility Enhancement Framework for IoT in Next Generation Cellular Networks,” *IEEE Access*, vol. 7, pp. 29 158–29 172, 2019.
- [34] G. Hattab and D. Cabric, “Energy-Efficient Massive IoT Shared Spectrum Access Over UAV-Enabled Cellular Networks,” *IEEE Transactions on Communications*, vol. 68, no. 9, pp. 5633–5648, 2020.
- [35] “Technical Specification Group Radio Access Network; NR; NR and NG-RAN Overall Description,” *3GPP TS 38.300 version 16.8.0*, Dec. 2021.
- [36] O. Liberg *et al.*, “Cellular Internet of Things: Technologies, Standards, and Performance,” *Academic Press*, 2017.
- [37] A. Baddeley, Ed., *Stochastic Geometry: Spatial Point Processes and Their Applications*. Berlin, Germany: Springer, 2007.
- [38] N. Abramson, “The ALOHA system: Another alternative for computer communications,” *Proc. Fall Joint Comput. Conf.*, Nov. 1970.
- [39] L. Kleinrock, “Queueing systems: Volume 1: Theory,” 1976.
- [40] T. Bonald, “The Erlang Model with non-Poisson Call Arrivals,” *Joint International Conference on Measurement and Modeling of Computer Systems*, Jun. 2006.
- [41] L. C. E. R. R. L. S. C. Cormen, T. H., “Introduction to algorithms (2nd ed.),” *MIT Press McGraw-Hill*, p. 344, 2001.